Journal of Sound and Vibration 333 (2014) 818–834

Contents lists available at ScienceDirect

Journal of Sound and Vibration

journal homepage: www.elsevier.com/locate/jsvi

Complex eigensolutions of coupled flexural and longitudinal modes in a beam with inclined elastic supports with non-proportional damping

Scott Noll, Jason Dreyer, Rajendra Singh *

Acoustics and Dynamics Laboratory, Smart Vehicle Concepts Center, Department of Mechanical Engineering, The Ohio State University, Columbus, Ohio 43210, USA

ARTICLE INFO

Article history:
Received 17 October 2012
Received in revised form
9 July 2013
Accepted 11 September 2013
Handling Editor: S. Ilanko
Available online 25 October 2013

ABSTRACT

Structure borne vibration and noise in an automobile are often explained by representing the full vehicle as a system of elastically coupled beam structures representing the body, engine cradle and body subframe where the engine is often connected to the chassis via inclined viscoelastic supports. To understand more clearly the interactions between a beam structure and isolators, this article examines the flexural and longitudinal motions in an elastic beam with intentionally inclined mounts (viscoelastic end supports). A new analytical solution is derived for the boundary coupled Euler beam and wave equations resulting in complex eigensolutions. This system is demonstrated to be self-adjoint when the support stiffness matrices are symmetric; thus, the modal analysis is used to decouple the equations of motion and solve for the steady state, damped harmonic response. Experimental validation and computational verifications confirm the validity of the proposed formulation. New and interesting phenomena are presented including coupled rigid motions, modal properties for ideal angled roller boundaries, and relationships between coupling and system modal loss factors. The ideal roller boundary conditions when inclined are seen as a limiting case of coupled longitudinal and flexural motions. In particular, the coupled rigid body motions illustrate the influence of support stiffness coupling on the eigenvalues and eigenfunctions. The relative modal strain energy concept is used to distinguish the contribution of longitudinal and flexural deformation modes. Since the beam is assumed to be undamped, the system damping is derived from the viscoelastic supports. The support damping (for a given loss factor) is shown to be redistributed between the system modes due to the inclined coupling mechanisms. Finally, this article provides valuable insight by highlighting some technical issues a real-life designer faces when balancing modeling assumptions such as rigid or elastic formulations, proportional or non-proportional damping, and coupling terms in multi-dimensional joint properties.

1. Introduction

Eigensolutions of continuous beams or rods with non-ideal boundaries have fascinated researchers for decades. Indeed there is vast body of literature on stiffness or mass loading boundary conditions as evident by Gorman's book on the subject [1]. Pure viscously damped boundary conditions lead to complex modal solutions and the so-called traveling waves for eigenfunctions [2]. Non-ideal viscous boundary conditions are often examined with ideal displacement boundaries. For example, Hull [3] and Prater

* Corresponding author. Tel.: +1 614 292 9044.
E-mail address: singh.3@osu.edu (R. Singh).

0022-460X/$ - see front matter © 2013 Elsevier Ltd. All rights reserved.
http://dx.doi.org/10.1016/j.jsv.2013.09.013

et al. [4] examine a bar with one end clamped and the other with viscous boundary; Prater and Singh [2] and Oliveto et al. [5] analyze a beam in flexure with pinned and viscous boundary conditions. These approaches [2–5] separate the elastic and viscous boundary effects. Conversely, the literature on the effect of viscoelastic supports on beam vibration characteristics is rather sparse, as stated in the summary provided by Kang and Kim [6]. Viscoelastic boundaries for beam or plate structures are typically modeled as complex stiffness elements [6,7]. Finally, multidimensional boundary coupling between transverse and longitudinal motions has not attracted much attention though such coupling is found in many real-life joints and supports. Realistic elastomeric joints are complex structures; yet, they are often simplified in their representation in system models as spring stiffness values in principal directions. When viewed as a matrix, the diagonal terms are the principal stiffness values. Elastomeric joints and supports are widely used in vehicle isolation systems, and their geometries are usually shaped to provide favorable properties in certain directions based on the diagonal terms [8]. Nonetheless, non-diagonal (coupling) terms are often unknown though they are intrinsic to the design of complex automotive assemblies [9,10].

Non-self-adjoint problems commonly appear in structural dynamic system with circulatory, aerodynamic, or gyroscopic forces [11–13]. In these problems, the linear differential operator does not equal the adjoint operator. However, a system with a self-adjoint operator may be rendered non-self-adjoint due to the boundary conditions, a topic that has received little attention [14] and where conflicts appear in the open literature. For instance, Jovanic [14] describes the analytical formulation of a cantilever beam with the free end connected to a viscous damping element; this demonstrates that the system is non-self-adjoint due to the boundary conditions. Han and Zu [11] mistakenly claim that viscous damping cannot destroy the symmetry of the system and thus cannot be non-self-adjoint. Likewise, Fan et al. [7] demonstrate that an end supported beam with structural damping is self-adjoint, but this is implicitly based on a necessary condition that no boundary coupling between longitudinal and flexural vibrations exists. In view of these above mentioned limitations, this article attempts to fill this void and proposes to extend the formulation of Fan et al. [7] to include non-ideal, viscoelastic coupling between longitudinal and transverse motions of the beam.

2. Problem formulation

The conceptual problem formulation is illustrated in Fig. 1a where an elastic beam is end supported on arbitrarily shaped and inclined viscoelastic joints at $x=0$ and L. Kinematic and elastic coupling of the structural modes is introduced through the boundary conditions that couple the transverse $w(x,t)$, slope $\theta(x,t)$ and longitudinal $u(x,t)$ motions of the beam. The rigid body, transverse bending, and longitudinal vibrations (say up to 3500 Hz) are of concern. The supports are described by a lumped complex stiffness which is often used to model viscoelastic effects in elastomers. The damping at the end supports introduces non-proportional damping to the beam structure; thus complex eigensolutions are required [2,6,7].

The scope of the analytical formulation is limited to a uniform cross-section elastic beam structure connected to ground through two supports. The assembled system is assumed to be linear time-invariant. Fan et al. [7] raise the issue through physical reasoning of conditions required for self-adjoint properties for a beam system with uncoupled transverse and longitudinal motion; thus, the conditions for self-adjoint properties of the coupled system are examined. The specific objectives of this article are as follows: (1) extend the formulation of Fan et al. [7] to include coupling between longitudinal and transverse motions of the beam; (2) verify the analytical solution with a discrete finite element model based on the Euler theory and rigid body formulation, as well as with limited modal tests; (3) demonstrate the limiting case of ideal boundary conditions utilizing inclined roller supports to couple longitudinal and transverse displacements at the beam ends; and (4) examine the system loss factor and complexity of the eigensolution using a non-proportionality index. The

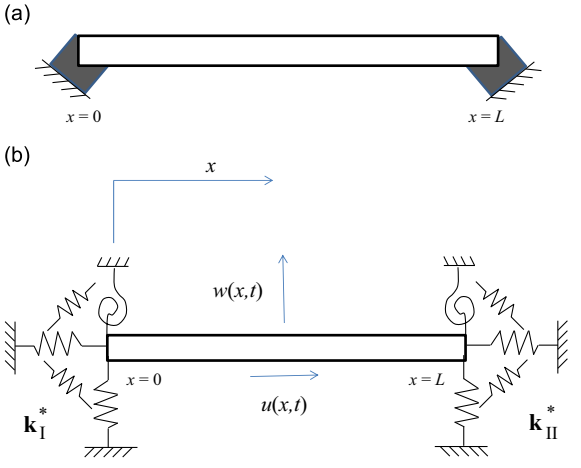

Fig. 1. Conceptual formulation of the end supported beam: (a) elastic beam is end supported by inclined viscoelastic supports; and (b) equivalent lumped complex stiffness representation of the viscoelastic supports, $\mathbf{k}_{\mathrm{I}}^{*}=\mathbf{k}_{\mathrm{I}}(1+\mathrm{i}\gamma_{\mathrm{I}})$ and $\mathbf{k}_{\mathrm{II}}^{*}=\mathbf{k}_{\mathrm{II}}(1+\mathrm{i}\gamma_{\mathrm{II}})$.

energy dissipated by the system is assumed to be dominated by the structural damping at the supports. The complex stiffness representation of the structural damping limits the analysis to the frequency domain and steady-state, damped sinusoidal response in the time domain.

For this article, the beam parameters are as follows: Young's modulus, $E=207$ GPa, Poisson's ratio, $\nu=0.3$, and mass density, $\rho=7850\ \mathrm{kg\,m^{-3}}$. The beam is 914 mm in length (L) with a rectangular cross-section of $25.4\times 50.8\ \mathrm{mm^2}$ where the thickness is 25.4 mm in the transverse direction. Certain automotive isolators are known to exhibit elastic coupling [10] and kinematic coupling is introduced through inclining the isolator. The lumped stiffness matrices for supports can take on any number of configurations that couple beam vibrations. The essential ingredient is to couple longitudinal motion with either the slope or transverse motion of the beam through one or a combination of elastic and kinematic coupling. For illustration purposes, this article will examine coupling introduced through kinematic inclination of isolators only, avoiding the unnecessary complication of assigning values for the elastic coupling. The supports have parameters of loss factor, γ, aspect ratio, R, non-dimensional stiffness, $\overline{k}$, and opposing inclination angles, θ; these are discussed later.

In vehicle handling and engine isolation applications, the rigid body modes are of critical importance, and it is convenient to analyze complicated assemblies at the lower frequencies by assuming that the compliance in the system is mostly confined to the jointed locations. For this article, the rigid body formulation is developed for three reasons. First, it offers a clear visualization of the coupling of vibration modes allowing one to gain some physical intuition into the problem. Second, the rigid body formulation provides a verification of the flexible formulation for low ratios of support to structure stiffness. Finally, through comparison with the flexible formulation, a designer may gain insight to errors that may occur when the assumption of rigid body motion is no longer valid.

3. Analytical solution of coupled beam motions

3.1. Complex eigensolution

The governing equations for a beam in longitudinal and transverse motion according to the Euler beam theory and wave equation in matrix form is

$$M\ddot{\mathbf{q}}+\mathbf{K}\mathbf{q}=\mathbf{p} \tag{1}$$

where $\mathbf{q}=[w(x,t)\ u(x,t)]^{\mathrm{T}}$ is the displacement vector, $\mathbf{M}$ is the mass operator,

$$\mathbf{M}=\begin{bmatrix}\mu(x) & 0\\ 0 & \mu(x)\end{bmatrix}, \tag{2}$$

where μ is the mass per unit length. $\mathbf{K}$ is the stiffness operator defined as

$$\mathbf{K}=\begin{bmatrix}EI\mathrm{d}^4/\mathrm{d}x^4 & 0\\ 0 & -EA\mathrm{d}^2/\mathrm{d}x^2\end{bmatrix} \tag{3}$$

where E is Young's modulus, I is the area moment of inertia, and A is the cross-sectional area. The sinusoidal load vector, $\mathbf{p}$ is of the form

$$\mathbf{p}=\begin{bmatrix}f_w & f_u\end{bmatrix}^{\mathrm{T}}=\mathbf{p}(x)\mathrm{e}^{\mathrm{i}\omega t}. \tag{4}$$

The equations of motion (1) are coupled through the stiffness boundary conditions at $x=0$,

$$\begin{bmatrix}EA\frac{\partial u(0,t)}{\partial x} & -EI\frac{\partial^3 w(0,t)}{\partial x^3} & EI\frac{\partial^2 w(0,t)}{\partial x^2}\end{bmatrix}^{\mathrm{T}}=\mathbf{k}_{\mathrm{I}}\begin{bmatrix}u(0,t) & w(0,t) & \frac{\partial w(0,t)}{\partial x}\end{bmatrix}^{\mathrm{T}} \tag{5}$$

and at $x=L$,

$$\begin{bmatrix}-EA\frac{\partial u(L,t)}{\partial x} & EI\frac{\partial^3 w(L,t)}{\partial x^3} & EI\frac{\partial^2 w(L,t)}{\partial x^2}\end{bmatrix}^{\mathrm{T}}=\mathbf{k}_{\mathrm{II}}\begin{bmatrix}u(L,t) & w(L,t) & -\frac{\partial w(L,t)}{\partial x}\end{bmatrix}^{\mathrm{T}}. \tag{6}$$

Here $\mathbf{k}_{\mathrm{I}}$ and $\mathbf{k}_{\mathrm{II}}$ are arbitrary lumped complex stiffness matrices of dimension 3. Assuming a separable solution, the complex eigenfunctions to the boundary valued problem are of the following form where r is the modal index:

$$\mathbf{\Psi}_r=\begin{bmatrix}W_r & U_r\end{bmatrix}^{\mathrm{T}} \tag{7}$$

where

$$U_r(x)=a_{1r}\ \sin(\beta_u x)(+a_{2r}\ \cos(\beta_u x) \tag{8}$$

$$W_r(x)=a_{3r}\ \sin(\beta_w x)+a_{4r}\ \cos(\beta_w x)+a_{5r}\ \sinh(\beta_w x)+a_{6r}\ \cosh(\beta_w x). \tag{9}$$

Here $\beta_u = \lambda_r\sqrt{\mu/EA}$ and $\beta_w = \sqrt[4]{\mu\lambda_r^2/EI}$ according to wave equation and the Euler beam theory [15], respectively. The complex valued eigenvalues, λ_r, are found by the frequency matrix as

$$\det(\boldsymbol{\Theta}(\lambda_r)) = 0. \tag{10}$$

The elements of $\boldsymbol{\Theta}(\lambda_r)$ are provided in Table 1. The transcendental equation, $\det(\boldsymbol{\Theta}(\lambda_r)) = 0$, must be numerically solved for λ_r [6,7]. Once the eigenvalues are obtained, the complex valued coefficients of the eigenfunctions, $\mathbf{a}_r$, as defined by Eqs. (8) and (9) are determined by a set of simultaneous equations:

$$\boldsymbol{\Theta}(\lambda_r)\mathbf{a}_r = \{0\}. \tag{11}$$

3.2. Requirements for self-adjoint properties

For the linear system shown in Eq. (1) to be considered self-adjoint, the following conditions must hold [15]:

$$\int_0^L \boldsymbol{\Psi}_m^{\mathrm{T}}\mathbf{k}\boldsymbol{\Psi}_n \mathrm{d}x = \int_0^L \boldsymbol{\Psi}_n^{\mathrm{T}}\mathbf{K}\boldsymbol{\Psi}_m \mathrm{d}x \tag{12}$$

and

$$\int_0^L \boldsymbol{\Psi}_m^{\mathrm{T}}\mathbf{M}\boldsymbol{\Psi}_n \mathrm{d}x = \int_0^L \boldsymbol{\Psi}_n^{\mathrm{T}}\mathbf{M}\boldsymbol{\Psi}_m \mathrm{d}x. \tag{13}$$

Eq. (13) satisfies the requirement for the beam since it expands into:

$$\int_0^L \mu(W_m W_n + U_m U_n)\mathrm{d}x = \int_0^L \mu(W_n W_m + U_n U_m)\mathrm{d}x \tag{14}$$

whereas, Eq. (12) simplifies into

$$\int_0^L (EIW_m W_n'''' - EAU_m U_n'')\mathrm{d}x = \int_0^L (EIW_n W_m'''' - EAU_n U_m'')\mathrm{d}x, \tag{15}$$

requiring additional examination. Assuming constant values for A, E, and I, one can rewrite the following terms: $W_m W_n''''$, $W_n W_m''''$, $U_m U_n''$, and $U_n U_m''$, as

$$\int_0^L W_m W_n'''' dx = W_m W_n'''|_o^L - W_m' W_n''|_o^L + \int_0^L W_m'' W_n'' \mathrm{d}x \tag{16}$$

$$\int_0^L W_n W_m'''' dx = W_n W_m'''|_o^L - W_n' W_m''|_o^L + \int_0^L W_m'' W_n'' \mathrm{d}x \tag{17}$$

$$\int_0^L U_m U_n'' dx = U_m U_n'|_o^L - \int_0^L U_m' U_n' \mathrm{d}x \tag{18}$$

$$\int_0^L U_n U_m'' dx = U_n U_m'|_o^L - \int_0^L U_m' U_n' \mathrm{d}x \tag{19}$$

Table 1
Frequency matrix elements, Θ_{ij}.

i	j					
	1	2	3	4	5	6
1	$EA\beta_u$	$-k_{\mathrm{I},11}$	$-k_{\mathrm{I},13}\beta_w$	$-k_{\mathrm{I},12}$	$-k_{\mathrm{I},13}\beta_w$	$-k_{\mathrm{I},12}$
2	0	$-k_{\mathrm{I},21}$	$EI\beta_w^3 - k_{\mathrm{I},23}\beta_w$	$-k_{\mathrm{I},22}$	$-EI\beta_w^3 - k_{\mathrm{I},23}\beta_w$	$-k_{\mathrm{I},22}$
3	0	$-k_{\mathrm{I},31}$	$-k_{\mathrm{I},33}\beta_w$	$EI\beta_w^2 - k_{\mathrm{I},32}$	$-k_{\mathrm{I},33}\beta_w$	$EI\beta_w^2 - k_{\mathrm{I},32}$
4	$-EA\beta_u \cos(\beta_u L)$ $-k_{\mathrm{II},11}\sin(\beta_u L)$	$EA\beta_u \sin(\beta_u L)$ $-k_{\mathrm{II},11}\cos(\beta_u L)$	$-k_{\mathrm{II},12}\sin(\beta_w L)$ $+k_{\mathrm{II},13}\beta_w \cos(\beta_w L)$	$-k_{\mathrm{II},12}\cos(\beta_w L)$ $-k_{\mathrm{II},13}\beta_w \sin(\beta_w L)$	$-k_{\mathrm{II},12}\sinh(\beta_w L)$ $+k_{\mathrm{II},13}\beta_w \cosh(\beta_w L)$	$-k_{\mathrm{II},12}\cosh(\beta_w L)$ $+k_{\mathrm{II},13}\beta_w \sinh(\beta_w L)$
5	$-k_{\mathrm{II},21}\sin(\beta_u L)$	$-k_{\mathrm{II},21}\cos(\beta_u L)$	$-EI\beta_w^3\cos(\beta_w L)$ $-k_{\mathrm{II},22}\sin(\beta_w L)$ $+k_{\mathrm{II},23}\beta_w \cos(\beta_w L)$	$EI\beta_w^3\sin(\beta_w L)$ $-k_{\mathrm{II},22}\cos(\beta_w L)$ $-k_{\mathrm{II},23}\beta_w \sin(\beta_w L)$	$EI\beta_w^3\cosh(\beta_w L)$ $-k_{\mathrm{II},22}\sinh(\beta_w L)$ $+k_{\mathrm{II},23}\beta_w \cosh(\beta_w L)$	$EI\beta_w^3\sinh(\beta_w L)$ $-k_{\mathrm{II},22}\cosh(\beta_w L)$ $+k_{\mathrm{II},23}\beta_w \sinh(\beta_w L)$
6	$-k_{\mathrm{II},31}\sin(\beta_u L)$	$-k_{\mathrm{II},31}\cos(\beta_u L)$	$-EI\beta_w^2\sin(\beta_w L)$ $-k_{\mathrm{II},32}\sin(\beta_w L)$ $+k_{\mathrm{II},33}\beta_w \cos(\beta_w L)$	$EI\beta_w^3\sin(\beta_w L)$ $-k_{\mathrm{II},22}\cos(\beta_w L)$ $+k_{\mathrm{II},33}\beta_w \sin(\beta_w L)$	$EI\beta_w^2\sinh(\beta_w L)$ $-k_{\mathrm{II},32}\sinh(\beta_w L)$ $+k_{\mathrm{II},33}\beta_w \cosh(\beta_w L)$	$EI\beta_w^2\cosh(\beta_w L)$ $-k_{\mathrm{II},32}\cosh(\beta_w L)$ $+k_{\mathrm{II},33}\beta_w \sinh(\beta_w L)$

Substituting Eqs. (16)–(19) along with the boundary conditions, Eqs. (5) and (6), yield the following relationships for the left hand side of Eq. (15):

$$\begin{aligned}\int_0^L (EIW_m W_n'''' - EAU_m U_n'')\mathrm{d}x = \int_0^L (EIW_m'' W_n'' + EAU_m' U_n')\mathrm{d}x\\ + k_{I,11}U_m(0)U_n(0) + k_{I,12}U_m(0)W_n(0) + k_{I,13}U_m(0)W_n'(0)\\ + k_{I,21}W_m(0)U_n(0) + k_{I,22}W_m(0)W_n(0) + k_{I,23}W_m(0)W_n'(0)\\ + k_{I,31}W_m'(0)U_n(0) + k_{I,32}W_m'(0)W_n(0) + k_{I,33}W_m'(0)W_n'(0)\\ + k_{II,11}U_m(L)U_n(L) + k_{II,12}U_m(L)W_n(L) - k_{II,13}U_m(L)W_n'(L)\\ + k_{II,21}W_m(L)U_n(L) + k_{II,22}W_m(L)W_n(L) - k_{II,23}W_m(L)W_n'(L)\\ - k_{II,31}W_m'(L)U_n(L) - k_{II,32}W_m'(L)W_n(L) + k_{II,33}W_m'(L)W_n'(L)\end{aligned} \tag{20}$$

and for the right hand side of Eq. (15)

$$\begin{aligned}\int_0^L (EIW_n W_m'''' - EAU_n U_m'')\mathrm{d}x = \int_0^L (EIW_m'' W_n'' + EAU_m' U_n')\mathrm{d}x\\ + k_{I,11}U_m(0)U_n(0) + k_{I,12}U_n(0)W_m(0) + k_{I,13}U_n(0)W_m'(0)\\ + k_{I,21}W_n(0)U_m(0) + k_{I,22}W_m(0)W_n(0) + k_{I,23}W_n(0)W_m'(0)\\ + k_{I,31}W_n'(0)U_m(0) + k_{I,32}W_n'(0)W_m(0) + k_{I,33}W_n'(0)W_m'(0)\\ + k_{II,11}U_m(L)U_n(L) + k_{II,12}U_n(L)W_m(L) - k_{II,13}U_n(L)W_m'(L)\\ + k_{II,21}W_n(L)U_m(L) + k_{II,22}W_m(L)W_n(L) - k_{II,23}W_n(L)W_m'(L)\\ - k_{II,31}W_n'(L)U_m(L) - k_{II,32}W_n'(L)W_m(L) + k_{II,33}W_m'(L)W_n'(L).\end{aligned} \tag{21}$$

A close examination of Eqs. (20) and (21) reveals that the requirement for self-adjoint properties dictated by Eq. (12) is satisfied only when the support stiffness matrices are symmetric, i.e. $\mathbf{k}_{\mathrm{I}} = \mathbf{k}_{\mathrm{I}}^{\mathrm{T}}$ and $\mathbf{k}_{\mathrm{II}} = \mathbf{k}_{\mathrm{II}}^{\mathrm{T}}$.

3.3. Steady state harmonic vibration

For a self-adjoint system [15], it is known that:

$$\int_0^L \overline{\boldsymbol{\Psi}}_q^{\mathrm{T}} \mathbf{K} \overline{\boldsymbol{\Psi}}_r \mathrm{d}x = \lambda_q^2 \delta_{rq} \tag{22}$$

and

$$\int_0^L \overline{\boldsymbol{\Psi}}_q^{\mathrm{T}} \mathbf{M} \overline{\boldsymbol{\Psi}}_r \mathrm{d}x = \delta_{rq} \tag{23}$$

where δ_{rq} is the Kronecker delta function and the eigenfunctions are normalized, $\overline{\boldsymbol{\Psi}}_r = \begin{bmatrix} \overline{W}_r & \overline{U}_r \end{bmatrix}^{\mathrm{T}}$, with respect to $\mathbf{M}$. By using the modal expansion theorem, the steady-state solution can be assumed as

$$\begin{bmatrix} w(x,t) \\ u(w,t) \end{bmatrix} = \sum_{r=1}^{\infty} \overline{\boldsymbol{\Psi}}_r \xi_r(t). \tag{24}$$

Next, substituting Eq. (24) into Eq. (1) yields

$$\mathbf{M} \sum_{r=1}^{\infty} \overline{\boldsymbol{\Psi}}_r \ddot{\xi}_r + \mathbf{K} \sum_{r=1}^{\infty} \overline{\boldsymbol{\Psi}}_r \xi_r(t) = \mathbf{p}. \tag{25}$$

Multiplying Eq. (25) by $\overline{\boldsymbol{\Psi}}_q^{\mathrm{T}}$ and integrating over the domain:

$$\sum_{r=1}^{\infty} \ddot{\xi}_r \int_0^L \overline{\boldsymbol{\Psi}}_q^{\mathrm{T}} \mathbf{M} \overline{\boldsymbol{\Psi}}_r \mathrm{d}x + \sum_{r=1}^{\infty} \xi_r \int_0^L \overline{\boldsymbol{\Psi}}_q^{\mathrm{T}} \mathbf{k} \overline{\boldsymbol{\Psi}}_r \mathrm{d}x = \int_0^L \overline{\boldsymbol{\Psi}}_q^{\mathrm{T}} \mathbf{p} \mathrm{d}x \tag{26}$$

leads to the decoupled equations in the modal domain such that

$$\ddot{\xi}_q + \lambda_q^2 \xi_q = Q_q \mathrm{e}^{\mathrm{i}\omega t}, \quad q = 1, 2, \ldots \tag{27}$$

where

$$Q_q = \int_0^L \overline{\boldsymbol{\Psi}}_q^{\mathrm{T}} \mathbf{P} \mathrm{d}x. \tag{28}$$

The steady-state, damped harmonic response is written as follows where it is assumed that the starting transients would decay:

$$\begin{bmatrix} w(x,t) \\ u(w,t) \end{bmatrix} = \sum_{r=1}^{\infty} \overline{\Psi}_r \frac{Q_r}{\lambda_r^2 - \omega^2} e^{i\omega t} \tag{29}$$

4. Inclined non-ideal boundary supports

Consider two perpendicular complex support stiffness elements at each end of the beam. In matrix form, only diagonal elements exist such that:

$$\mathbf{k}_j^* = \begin{bmatrix} k_l & 0 & 0 \\ 0 & k_t & 0 \\ 0 & 0 & 0 \end{bmatrix} (1+i\gamma_j) = \overline{k}\frac{EI}{2L^3} \begin{bmatrix} R & 0 & 0 \\ 0 & 1 & 0 \\ 0 & 0 & 0 \end{bmatrix} (1+i\gamma_j). \tag{30}$$

where γ is the loss factor, $i=\sqrt{-1}$, the aspect ratio is defined as $R=k_l/k_t$, and the non-dimensional scaling parameter is $\overline{k}=k_tL^3/EI$. The terms of the joint stiffness matrices are normalized by the beam flexure stiffness parameter, EI/L^3, that appears in the finite element formulation shown later in this article. The kinematic coupling terms, k_{12} and k_{21}, between the longitudinal and transverse directions are introduced by inclining the supports to a specified angle, θ, computed by

$$k_{11} = R\cos^2(\theta) + \sin^2(\theta), \tag{31}$$

$$k_{22} = R\sin^2(\theta) + \cos^2(\theta), \tag{32}$$

$$k_{21} = k_{12} = (R-1)\sin(\theta)\cos(\theta). \tag{33}$$

When $R=1$, no kinematic coupling is introduced, i.e. $k_{21}=k_{12}=0$. Assuming that the end supports are diametrically opposed by an inward rotation of $\theta=45^\circ$, then the joint stiffness matrices are written as

$$\mathbf{k}_I^* = \overline{k}\frac{EI}{2L^3} \begin{bmatrix} R+1 & R-1 & 0 \\ R-1 & R+1 & 0 \\ 0 & 0 & 0 \end{bmatrix} (1+i\gamma_I), \quad \mathbf{k}_{II}^* = \overline{k}\frac{EI}{2L^3} \begin{bmatrix} R+1 & -R+1 & 0 \\ -R+1 & R+1 & 0 \\ 0 & 0 & 0 \end{bmatrix} (1+i\gamma_{II}). \tag{34a,b}$$

Note that the coupling elements for joint II (at the other end) exhibit negative values imposed by the kinematics. The reader is referred to Noll et al. [16] for a complete derivation of Eq. (31)–(34).

5. Rigid body formulation

Assuming a long, slender beam, the mass moment of inertia is $I_o = 1/12\, mL^2$. The equation of motion for the discrete rigid structure of dimension 3 at the rth mode is as follows:

$$\left[\lambda_r^2 m \begin{bmatrix} 1 & 0 & 0 \\ 0 & 1 & 0 \\ 0 & 0 & L^2/12 \end{bmatrix} + \overline{k}\frac{EI}{2L^3} \begin{bmatrix} 2(R+1) & 0 & L(1-R) \\ 0 & 2(R+1) & 0 \\ L(1-R) & 0 & (R+1)L^2/2 \end{bmatrix} (1+i\gamma) \right] \boldsymbol{\psi}_r = \mathbf{0} \tag{35}$$

where the modal vector, $\boldsymbol{\psi}_r = [\delta_u\ \delta_w\ \delta_\theta]^T$, is defined about the center of gravity. The second equation corresponding to $\delta_w(t)$ is uncoupled from the remaining equations, therefore its eigenvalue can be written simply; whereas, the remaining equations are solved by setting the determinant of the frequency matrix equal to zero and solving for $\lambda_{1,3}$ as

$$\lambda_{1,3} = \sqrt{\frac{2\overline{k}EI(1+i\gamma)}{mL^3}(R+1 \pm \sqrt{R^2-R+1})}, \quad \lambda_2 = \sqrt{\frac{\overline{k}EI(1+i\gamma)(R+1)}{mL^3}}. \tag{36}$$

Through substitution of the eigenvalues into the frequency matrix, the corresponding eigenvectors are solved for as

$$\boldsymbol{\psi}_{1,3} = \begin{bmatrix} \frac{L(1-R)}{2(R+1\pm 2\sqrt{R^2-R+1})} & 0 & 1 \end{bmatrix}^T, \quad \boldsymbol{\psi}_2 = \begin{bmatrix} 0 & 1 & 0 \end{bmatrix}^T. \tag{37}$$

Note that the eigenvectors are real, even though the supports include a complex stiffness in the formulation. The uncoupled eigenvectors, for $R=1$, consist of $\boldsymbol{\psi}_1 = [1\ \ 0\ \ 0]^T$, longitudinal translation; $\boldsymbol{\psi}_2 = [0\ \ 1\ \ 0]^T$, transverse translation; and $\boldsymbol{\psi}_3 = [0\ \ 0\ \ 1]^T$, rotational displacement about the center of gravity (Fig. 2). By selecting the opposing inclined support stiffness elements, the second eigenvector remains unchanged due to the canceling effects of the symmetrical non-ideal boundaries; whereas, the first and third eigenvectors ($r=1$ and 3) are coupled together. The coupled motion consists of both longitudinal and rotational motions; with eigenvector, $r=1$, has a center of rotation above the center of gravity. Conversely, the eigenvector $r=3$ has a center of rotation below the center of gravity. Also, the eigenvalues for $r=1$ and 3 differ from that of the uncoupled system (Fig. 3).

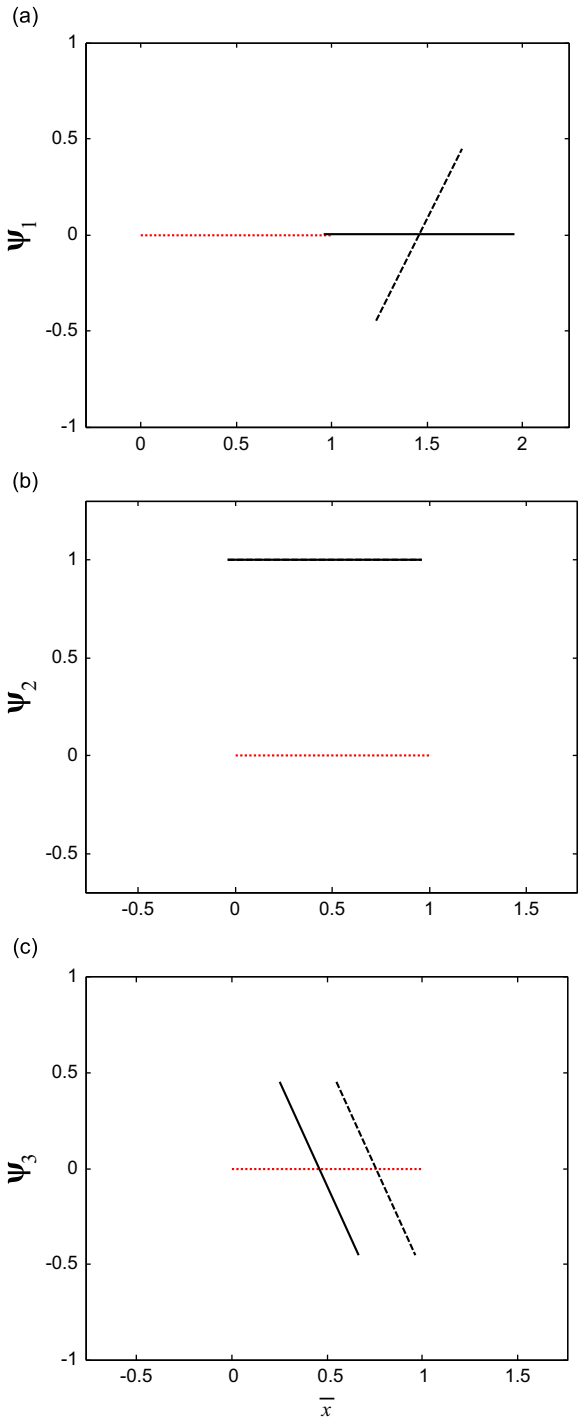

Fig. 2. Comparison of coupled and uncoupled rigid body modes, ψ_1 and ψ_3, plotted versus normalized coordinate, $\bar{x}$. Note that coupled and uncoupled modes, ψ_2, are identical. Key: — uncoupled; – – coupled; ——undisplaced position.

6. Computational verification and experimental validation

The analytical solutions of Sections 3.1 and 3.3 are verified with a computational beam model and the rigid body formulation. The computational model is comprised of 18 elements with lumped dynamic stiffness matrices at the end nodes and the formulation below is implemented into self-written script. A two-node Euler beam element is superposed with a longitudinal rod element to generate a two-node six degree of freedom element. This formulation assumes that

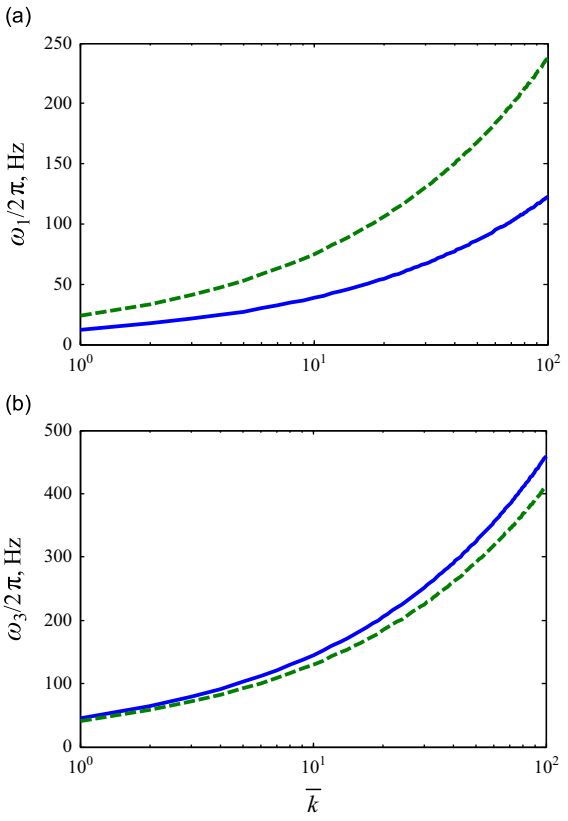

Fig. 3. Effect of coupling terms on the eigenvalues of a rigid beam with inclined end supports given $R=10$, and $\theta=45^\circ$: (a) $r=1$ and (b) $r=3$. Note: For $r=2$ (not shown), the eigenvalue remains unchanged since this is an uncoupled mode. Key: ▬ coupled mode; ▬ ▬ coupling terms (intentionally) ignored.

elastic longitudinal and beam bending are uncoupled. The work of Friedman and Kosmatka [17] contains a complete derivation of the finite element stiffness and mass matrices for a beam. The stiffness matrix for longitudinal degrees of freedom is written as

$$\mathbf{K}_l = \frac{EA}{L_e}\begin{bmatrix} 1 & -1 \\ -1 & 1 \end{bmatrix} \tag{38}$$

where L_e is the element length. The corresponding mass matrix for longitudinal motion is

$$\mathbf{M}_l = \frac{\rho A L_e}{6}\begin{bmatrix} 2 & 1 \\ 1 & 2 \end{bmatrix}. \tag{39}$$

The stiffness matrix for the Euler beam is

$$\mathbf{K}_b = \frac{EI}{L_e^3}\begin{bmatrix} 12 & 6L_e & -12 & 6L_e \\ 6L_e & 4{L_e}^2 & -6L_e & 2{L_e}^2 \\ -12 & -6L & 12 & -6L_e \\ 6L_e & 2{L_e}^2 & -6L_e & 4{L_e}^2 \end{bmatrix}, \tag{40}$$

where I is the area moment of inertia. The consistent mass matrix for the beam element is $\mathbf{M}_{bT}$ is associated with the translational inertia

$$\mathbf{M}_{bT} = \frac{\rho A L_e}{420}\begin{bmatrix} 156 & 22L_e & 54 & -13L_e \\ & 4{L_e}^2 & 13L_e & -3{L_e}^2 \\ & & 156 & -22L_e \\ \text{symmetric} & & & 4{L_e}^2 \end{bmatrix} \tag{41}$$

A validation experiment is also conducted using a steel beam (with Young's modulus, $E=207$ GPa, Poisson's ratio, $\nu=0.3$, and mass density, $\rho=7850$ kg m^{-3}, $L=914$ mm, $A=1290$ mm^2, thickness, $t=25.4$ mm). To introduce coupling, elastomeric cylinders are inclined at 45° from above and below the beam (Fig. 4a). The angled cylinders induce local coupling between the transverse and longitudinal movement of the beam at the joint. The elastomeric cylinders are specified as Neoprene

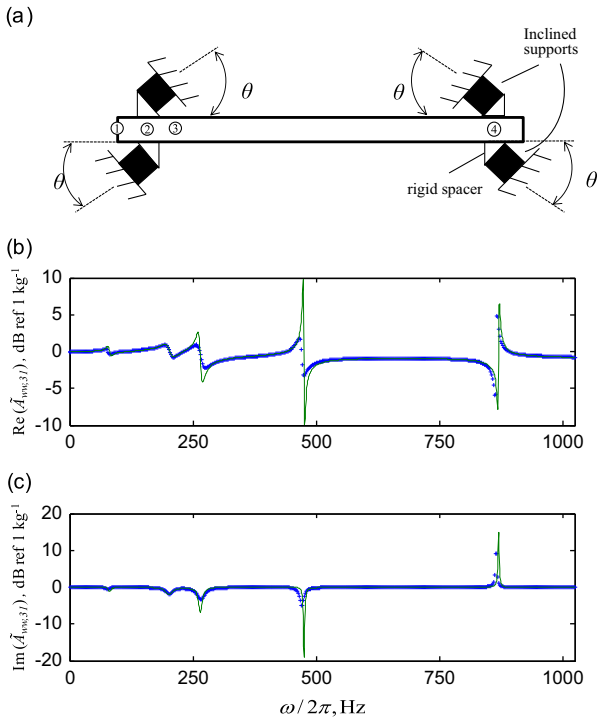

Fig. 4. Validation of computational beam model with modal experiment in terms of the cross point accelerance, $\tilde{A}_{ww,31}$, with excitation at point 1, $x=0$, and the response observed at point 3, $x=0.1$ m: (a) inclined supports located at point 2 and 4 are 0.05 m from the beam ends; (b) real part of $\tilde{A}_{ww,31}$; and (c) imaginary part of $\tilde{A}_{ww,31}$. Key: (+) modal experiment; (–) computational beam model.

with a Shore A hardness of 70. Accelerance measurements are taken on the beam with an accelerometer positioned at $x=0.1$ m and the impulse hammer applying a force input at $x=0$, both in the transverse (w) direction. Ten impacts at each location are averaged to minimize the random error in accelerance $\tilde{A}_{ij}(\omega)$ measurements. The multidimensional material properties of the support are documented in Noll et al. [16].

Since the experiment is supported at 0.05 m from each end of the beam, a computational beam model is first used to simulate the experiment to validate the assumptions in analysis. Next, the analytical formulation is verified with a separate computational beam model simulating supports at $x=0$ and L. The comparison (Fig. 4b,c) between experimental and computational results for the transverse cross point exhibits good agreement, though some regions show discrepancies. Excellent agreement is, however, achieved between the analytical and computational models; the comparison of the steady-state harmonic solution utilizing the Euler beam theory is shown in Fig. 5 where the computational results are computed by a direct inversion of the system matrices. The system eigenvalues are compiled in Table 2. The beam parameters selected for the numerical examples have a length to thickness ratio greater than 30.

The rigid body formulation exhibits agreement with the flexible formulation at lower values of support stiffness and then the eigenvalues diverge at a transition regime that differs for each mode, r (Fig. 6). The abscissa and ordinate for the coupled eigenfunction plots are defined respectively, as

$$\hat{U}(x)=(x+U(x))/L \quad \text{and} \quad \hat{W}(x)=W(x)/L. \tag{42a,b}$$

A transition point is defined at a 10% difference in the observed eigenvalue between the two formulations; a comparison of eigenfunctions at both the transition point support stiffness is presented with that of $\bar{k}=1$ (Fig. 6). At the support transition point, the beam exhibits significant elastic deformation in the eigenfunction that contributes to the overall compliance of the system.

7. Limiting case of opposing inclined roller supports

At the limiting case for k_t and $k_l \to \infty$ from Eq. (30), the solution returns to the ideal boundary conditions of pinned end supports uncoupling the longitudinal and transverse beam vibration, as expected. Alternatively, consider the limiting case where $k_t \to \infty$ and $k_l \to 0$ and the inclination angle is permitted to vary (Fig. 7). The single stiffness support approaches a roller boundary condition as the stiffness continues to increase and the inclination angle imposes a restriction at the beam

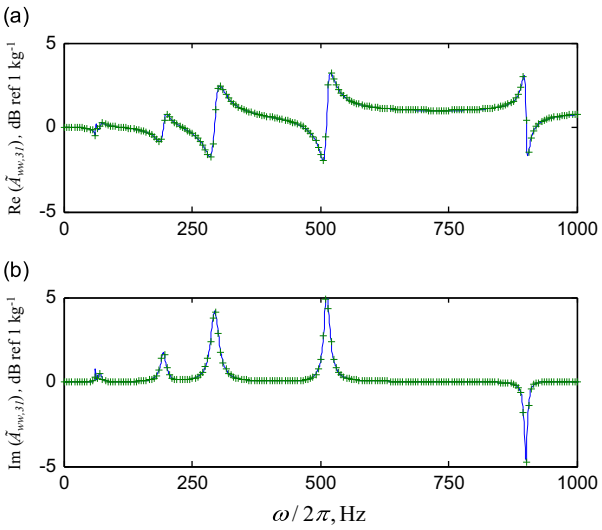

Fig. 5. Verification of analytical solution with computational beam model of the end supported beam in terms of the cross point accelerance, $\tilde{A}_{ww,31}$, with excitation at $x=0$ and the response observed at $x=0.1$ m: (a) real part of $\tilde{A}_{ww,31}$ and (b) imaginary part of $\tilde{A}_{ww,31}$. Key: (+) computational beam model; (–) proposed analytical solution.

Table 2
Comparison of first ten eigenvalues for the supported elastic beam ($R=7.2$, $\gamma=0.1$, $\theta=45$, $\bar{k}=34$).

Mode index r	Analytical model, Euler $\omega_r(1+i\eta_r)^{1/2}/2\pi$ (Hz)		Computational model, Euler $\omega_r(1+i\eta_r)^{1/2}/2\pi$ (Hz)	
	ω_r	η_r	ω_r	η_r
1	62	0.02	62	0.02
2	71	0.10	71	0.10
3	194	0.07	194	0.07
4	294	0.07	294	0.07
5	513	0.03	512	0.03
6	901	0.01	901	0.01
7	1453	0.00	1453	0.00
8	2153	0.00	2154	0.00
9	2812	0.00	2816	0.00
10	2997	0.00	3000	0.00

ends. Namely, the ratio of longitudinal and transverse translations remains at a constant value. Formally, at $x=0$,

$$\frac{w(0,t)}{u(0,t)} = -\tan(0.5\pi-\theta). \tag{43}$$

Additionally, the direction of the force at the beam end is known, such that the ratio of longitudinal and transverse forces is also a constant value:

$$\frac{-EI\frac{\partial^3 w(0,t)}{\partial x^3}}{EA\frac{\partial u(0,t)}{\partial x}} = \frac{-I\frac{\partial^3 w(0,t)}{\partial x^3}}{A\frac{\partial u(0,t)}{\partial x}} = \tan(0.5\pi-\theta). \tag{44}$$

Finally, the moment at $x=0$ vanishes:

$$EI\frac{\partial^2 w(0,t)}{\partial x^2} = 0. \tag{45}$$

Similarly, the boundary conditions at $x=L$ can be written as

$$\frac{-I(\partial^3 w(L,t)/\partial x^3)}{A(\partial u(L,t)/\partial x)} = -\tan(\pi/2-\theta),\quad \frac{w(L,t)}{u(L,t)} = \tan(\pi/2-\theta),\ \text{and}\ EI\frac{\partial^2 w(L,t)}{\partial x^2} = 0. \tag{46a–c}$$

With the new boundary conditions, a new frequency matrix is compiled (see Appendix A) from which the free and harmonic excitation solutions are solved using the procedures in Sections 3.1 and 3.3. The limiting case is verified with both the analytical and computation beam models by permitting $k_t \to 10^{12}$ and $k_l \to 0$ and the opposing inclination angles, $\theta=45^\circ$. The inclined roller supports permit rigid motion for combined longitudinal translation and rotation. This appears as a tilting in the modes shapes, noticeable in $r=2$ and 4 in Fig. 8. The eigenvalues are most similar to pinned–pinned boundary

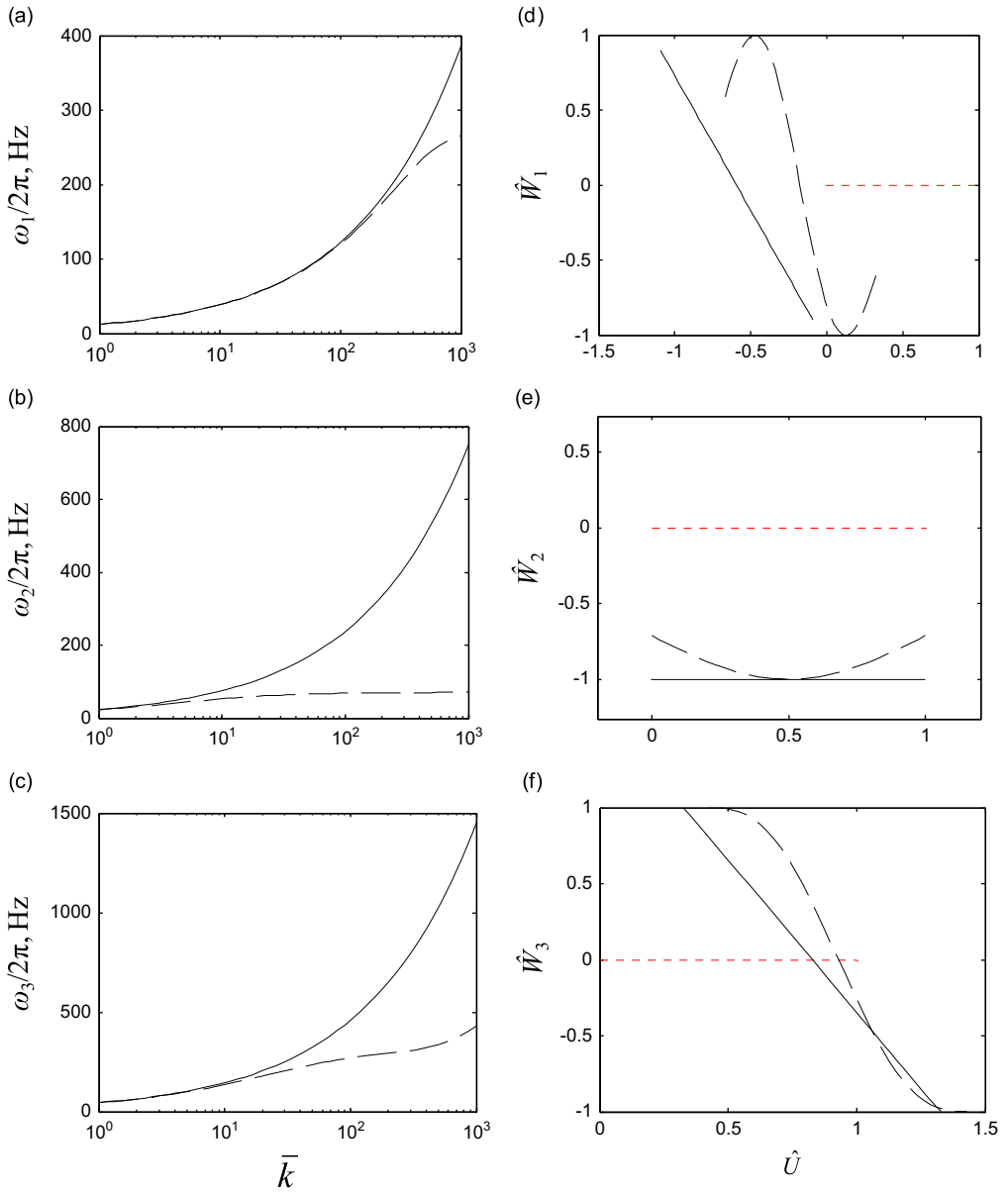

Fig. 6. Modal mapping of $\bar{k}$ illustrating the need for a flexible body formulation with $R=10$, $\theta=45^\circ$, and $\gamma=0$. Undamped eigenvalues versus $\bar{k}$ for (a) $r=1$; (b) $r=2$; (c) $r=3$. Key (a)–(c): — with rigid body formulation; – – elastic body formulation; eigenfunctions for (d) $r=1$; (e) $r=2$; (f) $r=3$. Key (d)–(f): — $\bar{k}=10^{-3}$; — — $\bar{k}$ selected at transition point defined at an observed 10% difference in the eigenvalue.

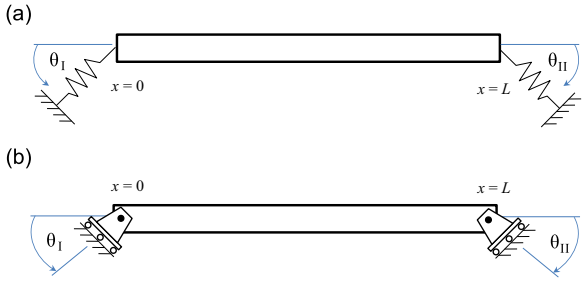

Fig. 7. Limiting case of the boundary support as $\bar{k}\to\infty$. (a) single inclined lumped spring support and (b) angled (ideal) roller boundary conditions, i.e. $\bar{k}=\infty$.

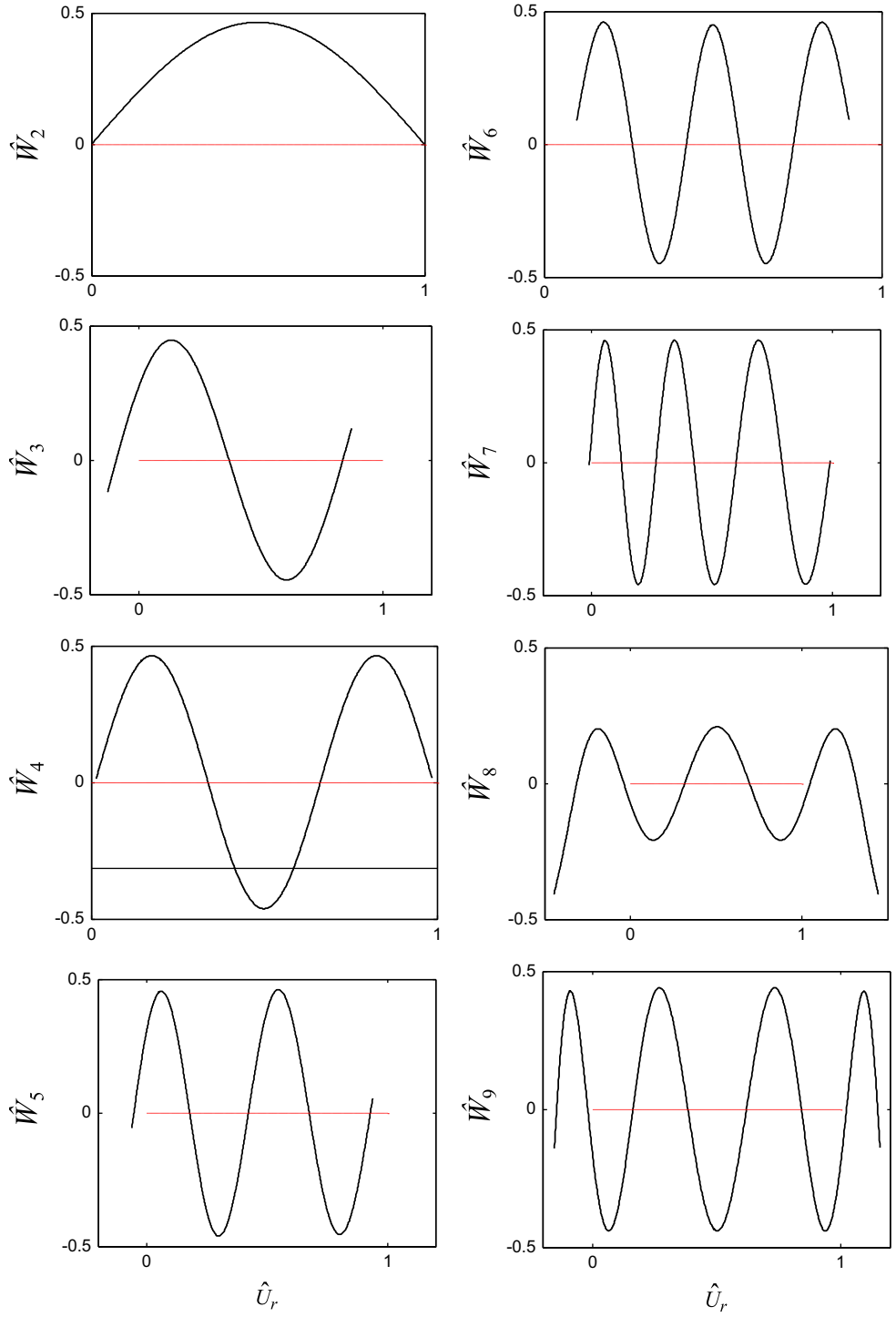

Fig. 8. Eigenfunctions for the limiting case of Fig. 7 with inclined roller boundary supports at $\theta=45^\circ$.

conditions (see Table 3) except when significant coupling is observed. The modal strain energy, Π_r, provides a coupling metric for each mode of the energy stored in longitudinal and bending deflection (Table 4). Here, the modal strain energy for the flexural deflection is defined as

$$\Pi_{b,r} = 0.5EI \int_0^L (\partial^2 W_r/\partial x^2)^2 \mathrm{d}x \tag{47}$$

Table 3
Comparison of first nine eigenvalues for ideal boundary supports for an elastic beam ($\omega_r/2\pi$, Hz).

Mode index r	Beam flexure free–free	Beam flexure pinned–pinned	Limiting coupled case: angled roller	Longitudinal free–free
1	0	71	0	0
2	0	283	71	0
3	0	636	307	0
4	160	1131	633	2807
5	442	1768	1154	5614
6	867	2546	1724	–
7	1432	3465	2551	–
8	2139	–	2644	–
9	2988	–	3568	–

Table 4
Strain energy ratio for the ideal angled roller boundary conditions of an elastic beam.

Mode index r	$\Pi_{b,r}/\Pi_{\text{Total}}$	$\Pi_{l,r}/\Pi_{\text{Total}}$
1	–	–
2	1.00	0.00
3	1.00	0.00
4	0.99	0.01
5	0.99	0.01
6	0.92	0.08
7	0.97	0.03
8	0.18	082
9	0.90	0.10

and for longitudinal deflection as

$$\Pi_{l,r} = 0.5AE \int_0^L (\partial U_r/\partial x)^2 \mathrm{d}x. \tag{48}$$

Significant coupling of the modes in Table 4 is first evident at ψ_6, where the ratios of strain energy are 92% and 8% stored in flexural and longitudinal vibration, respectively.

8. Modal damping and extent of non-proportionality

The structurally damped supports provide damping to the entire beam system; however, the damping is observed at varying levels at each mode of vibration. At low stiffness values, $\overline{k} < 1$, the rigid body modes take on a modal loss factor equal to or nearly equal to that of the support loss factor, that is the normalized modal loss factor, $\overline{\eta} = \eta/\gamma$, is equal to unity (Fig. 9). This result agrees with the prior work of Kang and Kim [6]. Interestingly though, their [6] uncoupled solution exhibited a single local maximum value for the first three modes; whereas the coupled solution presented in this article shows multiple peaks. Physically, the significance here is that this result demonstrates the possibility to intelligently select the multidimensional support properties for a given application to enhance damping at specific frequencies. At moderate to high values of support stiffness ($10 < \overline{k} < 10^5$), the elastic modes achieve their peak modal loss factor, however, at a fraction of the support loss factors. For $r=4$ to 6, the peak $\overline{\eta}$ falls into a range of 0.4–0.6; whereas modes $r=7$–9 achieve a peak $\overline{\eta}$ in the range of 0.1–0.4.

The beam system is non-proportionally damped with the structural damping elements at the end supports, thus complex eigenfunctions are required. The degree of complexity or the non-proportionality is of practical concern as in many applications it is convenient to assume normal modes. In this article, the metric for eigenfunction complexity proposed by Prater and Singh [2] is adopted where the non-proportionality index, δ_r, is defined as

$$\delta_r = (\mathrm{Im}/\mathrm{Re})_r \ (0 < (\mathrm{Im}/\mathrm{Re})_r < 1), \tag{49}$$

or

$$\delta_r = 1/(\mathrm{Im}/\mathrm{Re})_r \ (\mathrm{Im}/\mathrm{Re})_r > 1, \tag{50}$$

where

$$(\mathrm{Im}/\mathrm{Re})_r = \max\left\{\left|\mathrm{Im}\left(\begin{bmatrix} U_r(x) \\ W_r(x) \end{bmatrix}\right)\right|\right\} \Big/ \max\left\{\left|\mathrm{Re}\left(\begin{bmatrix} U_r(x) \\ W_r(x) \end{bmatrix}\right)\right|\right\}. \tag{51}$$

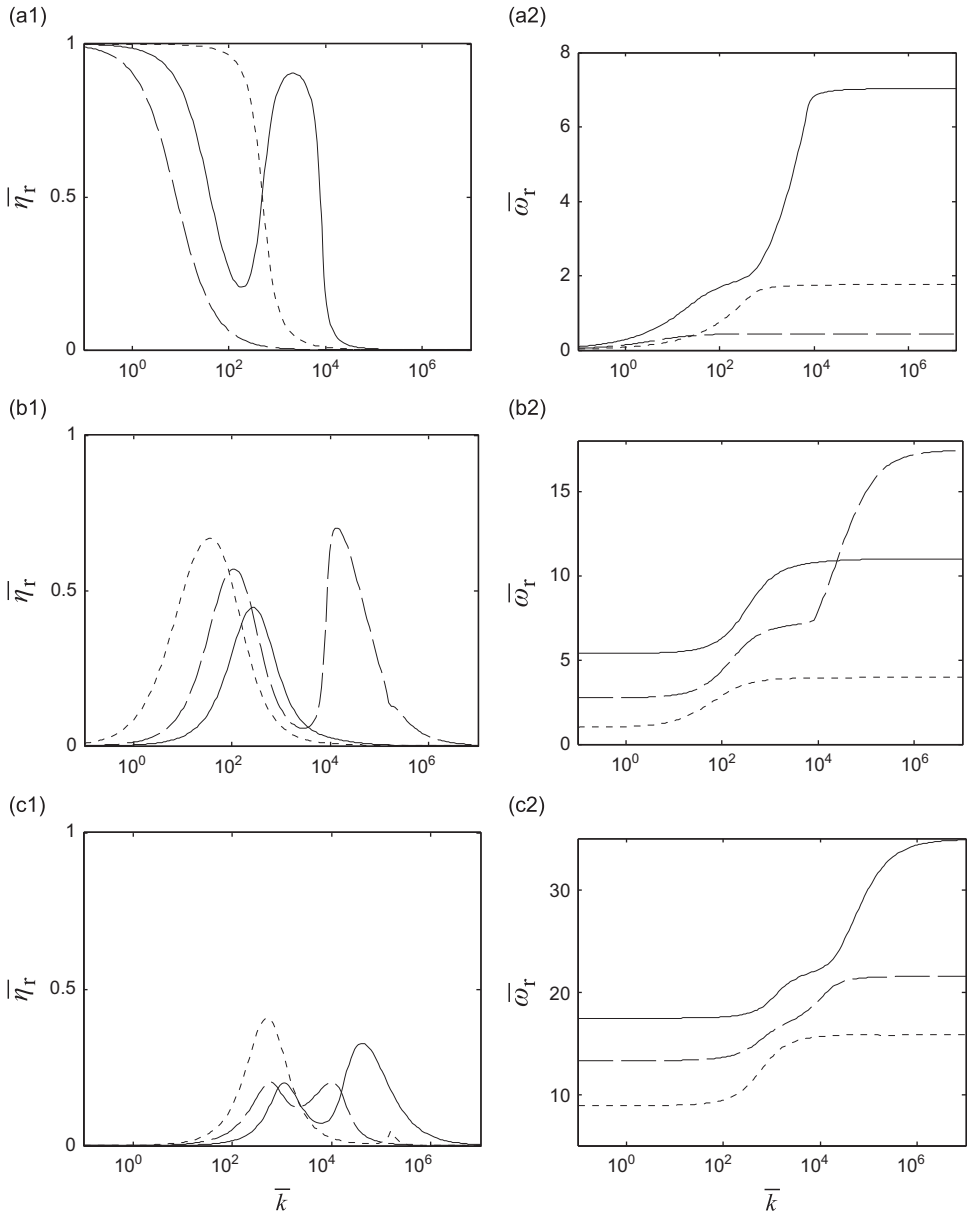

Fig. 9. Mapping of modal loss factor, $\overline{\eta}_r$, and natural frequency, $\overline{\omega}_r$, versus support stiffness $\overline{k}$. All values are normalized. Key: (a) rigid body modes, …$r=1$; --- $r=2$; –$r=3$; (b) elastic body modes, …$r=4$; --- $r=5$; –$r=6$; and (c) elastic body modes, –$r=7$; --- $r=8$; –$r=9$.

The non-proportionality index will take on values between 0 and 1, with a value of zero indicating undamped or proportional damping, whereas a value of 1 indicates equal value of the imaginary to real components of the eigenfunction typical of a heavily non-proportionally damped system.

The rigid body formulation predicts normal modes, and this result agrees with the elastic formulation for small values of $\overline{k}$ where $\delta_r=0$. Nominally, the peak value of δ_r for each mode falls in the range of 0.18–0.45 (Fig. 10) occurring at different values of $\overline{k}$. This means that for a given value of $\overline{k}$ the assumption of normal modes may be valid for certain modes and invalid for others. To clarify further, the real and imaginary components of the eigenfunctions are plotted in Fig. 11 for $\overline{k}=500$ with a spatial resolution of 5 mm. When the components of the eigenfunction form a straight line, such as the case Fig. 11b, the assumption of normal modes is valid; whereas, the components form an ellipse in Fig. 11c indicating a highly complex mode.

9. Conclusion

This article contributes to the state of the art by providing a new investigation and improved understanding of the modal properties of a non-proportionally damped beam with viscoelastic supports that couple its end motions. New expressions

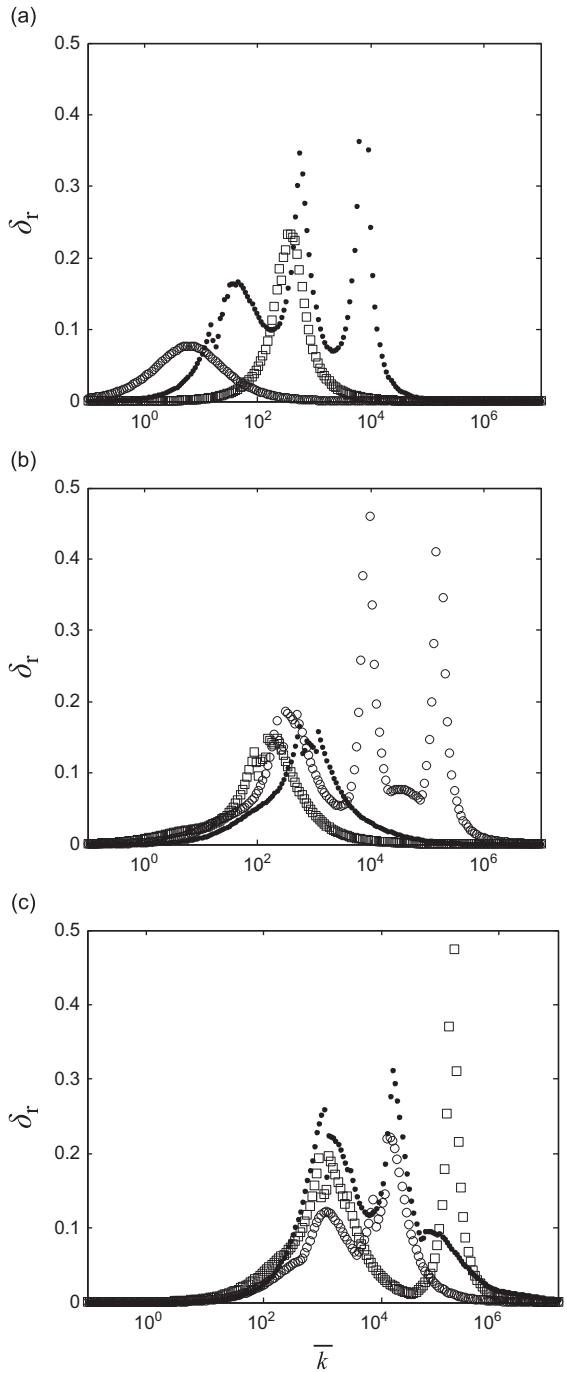

Fig. 10. Modal complexity index, δ, versus support stiffness, $\overline{k}$. Key: (a) rigid body modes, □ $r=1$; o $r=2$; • $r=3$; (b) elastic body modes, □ $r=4$; o $r=5$; • $r=6$; and (c) elastic body modes, □ $r=7$; o $r=8$; • $r=9$.

for exact eigensolution and steady-state harmonic response are given for the longitudinal and transverse Euler beam vibrations that are coupled through viscoelastic boundary supports. The most elementary case of coupled rigid body modes demonstrates that coupling influences both eigenvalues and eigenfunctions as well as highlights stiffness coupling concepts. The limiting case of inclined ideal roller boundary conditions clearly illustrates coupling between longitudinal and flexural eigenfunctions and the relative modal strain energy metric captures the contribution of elastic deformation. Also, it is shown that, unlike the uncoupled case formulated in prior work [6], coupling introduced through the supports can provide multiple local peak values for system modal loss factors.

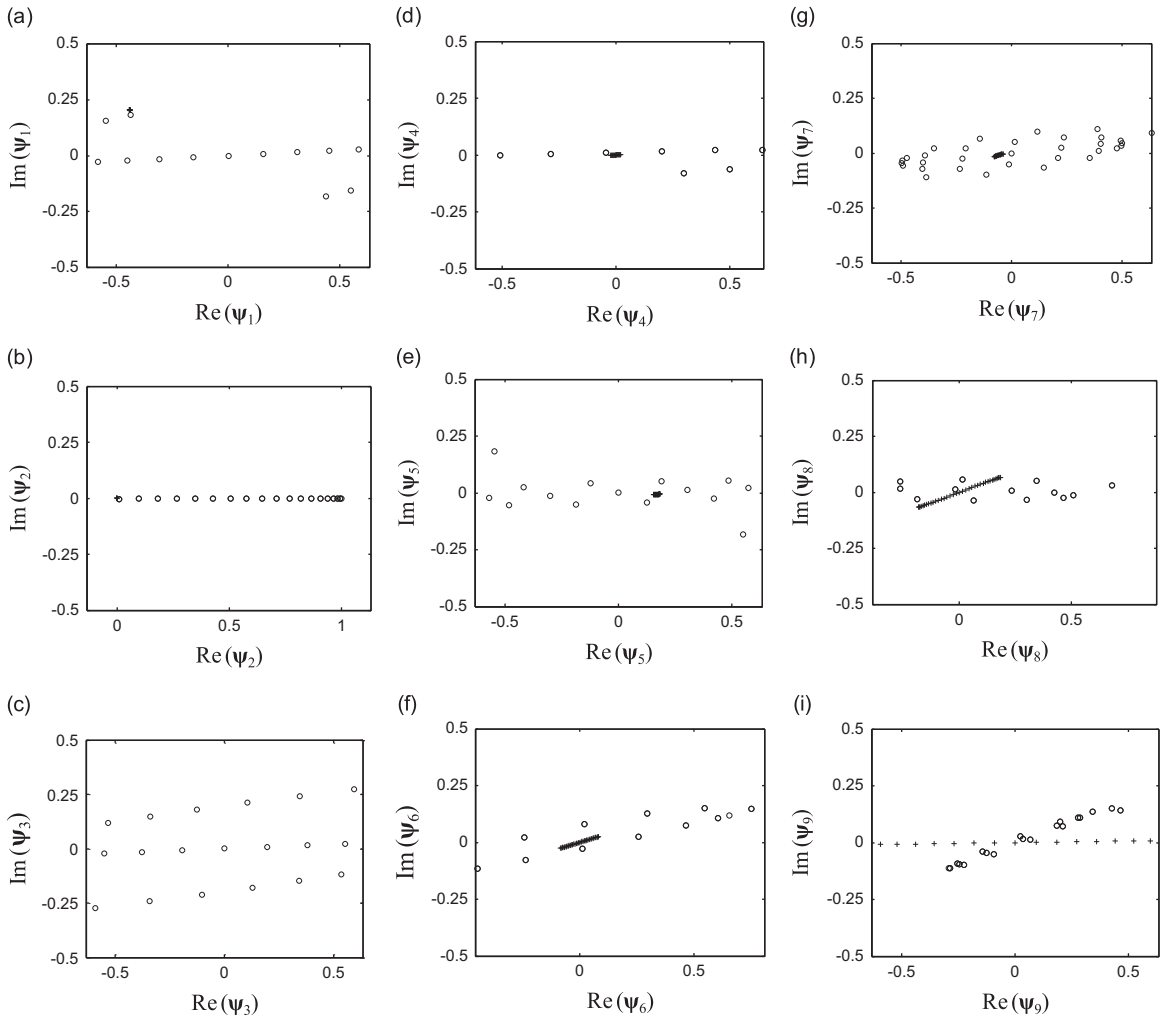

Fig. 11. Imaginary versus real parts of the eigenfunctions, ψ_r, with spatial resolution of 5 mm in the x-direction given $\overline{k} = 500$. Key: o w displacement; $+u$ displacement.

The flexural formulation has been limited to the Euler beam theory and that the supports were assumed to contain structural damping; viscous damping mechanism is not included. The parameters selected for the investigation meet the assumptions of the Euler beam theory; however, one must consider the rotary inertia and shear deformation in short beams in accordance with the Timoshenko beam theory. Also, the compliant supports are assumed to contain symmetric stiffness matrices, a property required to satisfy the conditions for self-adjoint properties. Although the problem is formulated with an end supported beam, the article provides valuable insight to the underlying physical phenomenon associated with real world assemblies that utilize shaped isolators in the supports or joints by considering non-diagonal terms in the support stiffness matrix that are intrinsic to the design in automotive isolation components. Finally, the many technical issues one faces when balancing the modeling assumptions for real world assemblies are highlighted. Specifically, examples between rigid body versus elastic body formulations, uncoupled versus coupled, and proportionally versus non-proportional damping provide some guidelines.

Acknowledgment

We acknowledge the member organizations such as Transportation Research Center Inc., Honda R&D Americas, Inc., YUSA Corporation and F.tech of the Smart Vehicle Concepts Center (www.SmartVehicleCenter.org) and the National Science Foundation Industry/University Cooperative Research Centers program (www.nsf.gov/eng/iip/iucrc) for supporting this work.

Table A1
Frequency matrix for limiting case of angled roller (ideal) boundary conditions, Θ_{ij}.

i	j					
	1	2	3	4	5	6
1	0	$\tan(0.5\pi-\theta)$	0	1	0	1
2	0	0	0	1	0	-1
3	$A\beta_u/I\beta_w^3\ \tan(0.5\pi-\theta)$	0	-1	0	1	0
4	$\beta_u\ \cos(\beta_u L)\tan(0.5\pi-\theta)$	$-\beta_u\ \sin(\beta_u L)\tan(0.5\pi-\theta)$	$(I\beta_w^3/A)\cos(\beta_w L)$	$(-I\beta_w^3/A)\sin(\beta_w L)$	$(-I\beta_w^3/A)\cosh(\beta_w L)$	$(-I\beta_w^3/A)\sinh(\beta_w L)$
5	$-\sin(\beta_u L)\tan(0.5\pi-\theta)$	$-\cos(\beta_u L)\tan(0.5\pi-\theta)$	$\sin(\beta_w L)$	$\cos(\beta_w L)$	$\sinh(\beta_w L)$	$\cosh(\beta_w L)$
6	0	0	$-\sin(\beta_w L)$	$-\cos(\beta_w L)$	$\sinh(\beta_w L)$	$\cosh(\beta_w L)$

Appendix A

See Table A1.

References

[1] D.J. Gorman, *Free Vibration Analysis of Beams and Shafts*, John Wiley & Sons, New York, 1975.
[2] G. Prater, R. Singh, Eigenproblem formulation, solution and interpretation for non-proportionally damped continuous beams, *Journal of Sound Vibration* 143 (1990) 125–142.
[3] A. Hull, A closed form solution of a longitudinal bar with a viscous boundary condition, *Journal of Sound and Vibration* 169 (1994) 19–28.
[4] R. Singh, W.M. Lyons, G. Prater, Complex eigensolution for longitudinally vibrating bars with a viscously damped boundary, *Journal of Sound and Vibration* 133 (1989) 364–367.
[5] G. Oliveto, A. Santini, E. Tripodi, Complex modal analysis of a flexural vibrating beam with viscous end conditions, *Journal of Sound and Vibration* 200 (1997) 327–345.
[6] K.H. Kang, K.J. Kim, Modal properties of beams and plates on resilient supports with rotational and translational complex stiffness, *Journal of Sound and Vibration* 190 (1996) 207–220.
[7] Z.J. Fan, J.H. Lee, K.H. Kang, K.J. Kim, The forced vibration of a beam with viscoelastic boundary supports, *Journal of Sound and Vibration* 210 (1998) 673–682.
[8] C. Lewitzke, P. Lee, Application of elastomeric components for noise and vibration isolation in the automotive industry, SAE Paper 2001-01-1447, 2001.
[9] H.J. Kim, K.J. Kim, Effects of rotational stiffness of bushings on natural frequency estimation for vehicles by substructure coupling based on frequency response functions, *International Journal of Vehicle Noise and Vibration* 6 (2010) 215–229.
[10] S. Kim, R. Singh, Multi-dimensional characterization of vibration isolators over a wide range of frequencies, *Journal of Sound and Vibration* 245 (2001) 877–913.
[11] R. Han, J. Zu, Pseudo non-selfadjoint and non-selfadjoint systems in structural dynamics, *Journal of Sound and Vibration* 184 (1995) 725–742.
[12] L. Meirovitch, Control of non-self-adjoint distributed-parameter systems, *Journal of Optimization Theory and Applications* 47 (1985) 77–90.
[13] B. Yang, Integral formulas for non-self-adjoint distributed dynamic systems, *American Institute of Aeronautics and Astronautics Journal* 34 (1996) 2132–2139.
[14] V. Jovanovic, A Fourier series solution for the transverse vibration response of a beam with viscous boundary, *Journal of Sound and Vibration* 330 (2011) 1504–1515.
[15] S.S. Rao, *Vibration of Continuous Systems*, John Wiley & Sons, New Jersey, 2007.
[16] S. Noll, J.T. Dreyer, R. Singh, Identification of dynamic stiffness matrices of elastomeric joints using direct and inverse methods, *Mechanical Systems and Signal Processing* 39 (2013) 227–244.
[17] Z. Friedman, J. Kosmatka, An improved two-node Timoshenko beam finite element, *Computers and Structures* 47 (1993) 473–481.